PROCEEDINGS OF SPIE

SPIEDigitalLibrary.org/conference-proceedings-of-spie

Multi-step reinforcement learning for medical image super-resolution

Alix Bouffard, Mihaela Pop, Mehran Ebrahimi

Alix Bouffard, Mihaela Pop, Mehran Ebrahimi, "Multi-step reinforcement learning for medical image super-resolution," Proc. SPIE 12464, Medical Imaging 2023: Image Processing, 124641Y (3 April 2023); doi: 10.1117/12.2653655

SPIE.

Event: SPIE Medical Imaging, 2023, San Diego, California, United States

Multi-Step Reinforcement Learning for Medical Image Super-Resolution

Alix Bouffard[a], Mihaela Pop[b], and Mehran Ebrahimi[a]

[a]Ontario Tech University, Oshawa, Ontario, Canada
[b]Sunnybrook Research Institute, Toronto, Ontario, Canada

Abstract

We apply a multi-agent Reinforcement Learning (RL) algorithm to single image super-resolution (SISR). In the area of RL, intelligent agents take actions in an environment in order to maximize a cumulative reward. In our novel implementation, each agent chooses a particular action from a fixed action set comprised of existing local enhancement operators to update each pixel intensity value. The pixel-wise arrangement of agents enables the algorithm to increase the resolution of an image by choosing optimal pixel intensity values from each option in a content-aware manner. While previous implementations of the model on SISR use Generative Adversarial Network (GAN)-based algorithms, we demonstrate that local operators can produce promising improved results without relying on the additional overhead of using machine learning techniques for the action space. Notably, we apply the proposed method to medical images, whereas previous implementations focused on natural images.

Keywords: Super-Resolution, MRI, A3C (Asynchronous Advantage Actor Critic), Reinforcement Learning

1. INTRODUCTION

Higher quality Magnetic Resonance Images (MRI) are valuable for early detection and accurate diagnosis of various medical conditions. High spatial resolution of images is essential to provide detailed anatomical information and help radiologists with accurate quantitative analysis. Acquiring higher resolution MRI requires longer image acquisition times, which can be costly for the exam itself, or may not always be possible due to physical limitations of the imaging system/sequences or due to patient's advanced pathological condition. Super-resolution (SR) techniques are alternative ways to improve the spatial resolution of images by producing a high-resolution (HR) image given a Low-resolution (LR) measurement. There are two classes of super-resolution methods: single-image and multiple-image. Multiple-image super-resolution is based on acquiring up to sub-pixel information sourced from multiple low-resolution scans of the same subject and generally allows for higher reconstruction accuracy at the expense of overhead. This paper focuses on single-image super-resolution (SISR), where one high-resolution image is synthesized from one low-resolution image.

SR approaches to produce HR MRI are mostly categorized into reconstruction-based and learning-based methods. Reconstruction-based techniques use interpolation filtering methods such as bilinear, bicubic or lanczos.[1] They are among the first methods to tackle SISR problems. However, interpolated images blur or degrade important edge and texture information of images. Interpolation methods do not always use any supplementary information when approximating the HR solution and the recovery of high-frequency information can be difficult. High-frequency information is important for constructing important edges in the high-resolution approximation. Evidently, this leads to the development of Super Resolution (SR) algorithms[2–18] which synthesize missing high-resolution pixel information that is not explicitly found in the LR measurements.

SISR methods have been widely advanced by the breakthroughs in deep learning. Methods based on Generative Adversarial Networks (GANs)[19] are promising approaches for image generation and have been also used for SR.[20] GANs-based models show the increasing performance for SISR. Different architectures and loss functions aimed at improving the quality of the generated images using GANs have been proposed. Recent advances in the Super Resolution Generative Adversarial Network (SRGAN) are aimed to recover fine texture details and edge information even at large upscaling factors.[20]

In the area of Reinforcement Learning (RL), intelligent agents have to take actions in an environment in order to maximize a cumulative reward. In RL-based image enhancement,[21–24] using GANs for the action

Medical Imaging 2023: Image Processing, edited by Olivier Colliot, Ivana Išgum,
Proc. of SPIE Vol. 12464, 124641Y · © 2023 SPIE
1605-7422 · doi: 10.1117/12.2653655

space as previous implementations of Pixel-RL-SISR requires a large training dataset and extensive computing power compared to using local enhancement operators. In addition to being easier to conceptualize how the actions modify the image, local techniques perform similarly and predictably when given different subject matter compared to GANs which need to be developed for specific applications.[25,26] Previous implementations of the so-called "PixelRL" model towards SISR focused on natural colour images and used GAN-based SISR algorithms as part of their action space.[21–24] Here, we validate the applicability of such methods on medical images. Furthermore, we use local operators due to their ease of implementation in comparison to using additional neural networks which need to be trained on a per-domain basis.

2. METHODOLOGY

We train our proposed RL model[27] on the Automated Cardiac Diagnosis Challenge (ACDC) dataset (STACOM 2018),[28] which has been pre-processed such that all blank scans have been removed and all images have been either cropped or zero-padded to 256×256 depending on the original image's dimensions. The model was trained on 742 images and validated on forty images from the ACDC dataset for $16,384$ "episodes" in batches of 64 images. The subjects and corresponding scans were not split between validation and training datasets, i.e., complete subject scans were used for validation and training. Subjects used for validation were chosen randomly throughout the ACDC set. Upon loading the batch into the model, the images were blurred using a normalized 4×4 box filter, down-scaled by a factor of four in each direction and then up-scaled back to the original size using bicubic interpolation. The goal here is to improve the quality of the initial bicubic interpolation of LR images to obtain a HR image using RL. The pixel values were then normalized to be between 0 and 1 and the bit-depth was reduced from 32 to 8. During the training, data augmentation was used by splitting the input images into 64×64 patches which were reflected and rotated. This differs from the previous implementations, where images were processed one-by-one as they were queued to be fed to the model instead of being pre-processed on a per batch basis, as well as being 64×64 rather than 70×70. Each 64×64 input is then processed through nine possible actions in the action space.

The action space that was empirically chosen for super-resolution is as follows, (1) pixel value increment, (2) pixel value decrement, (3) no action, (4) unsharp masking, (5) Laplacian filter, (6) Gaussian blur, (7) box blur, (8) edge enhance filter, (9) sharpen filter, see Figure 1.

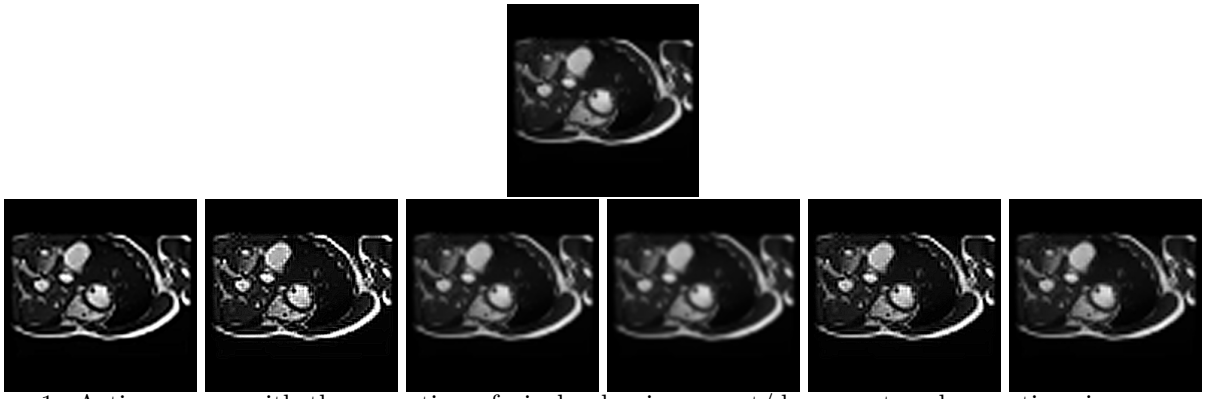

Figure 1: Action space, with the exception of pixel value increment/decrement and no action, in comparison with the input image, Top row: sample input taken from a sample of the ACDC dataset, Bottom row from left to right: Unsharp masking, Laplacian filter, Gaussian blur, box blur, edge enhance filter, and sharpen filter

Each pixel has its own "agent", which can then "decide" which action should be taken for that specific pixel to replace its current value. After each agent decides on an action, the new image is then used as the input for the next time step, the process is repeated four more times for a total episode length of five, see Figure 2.

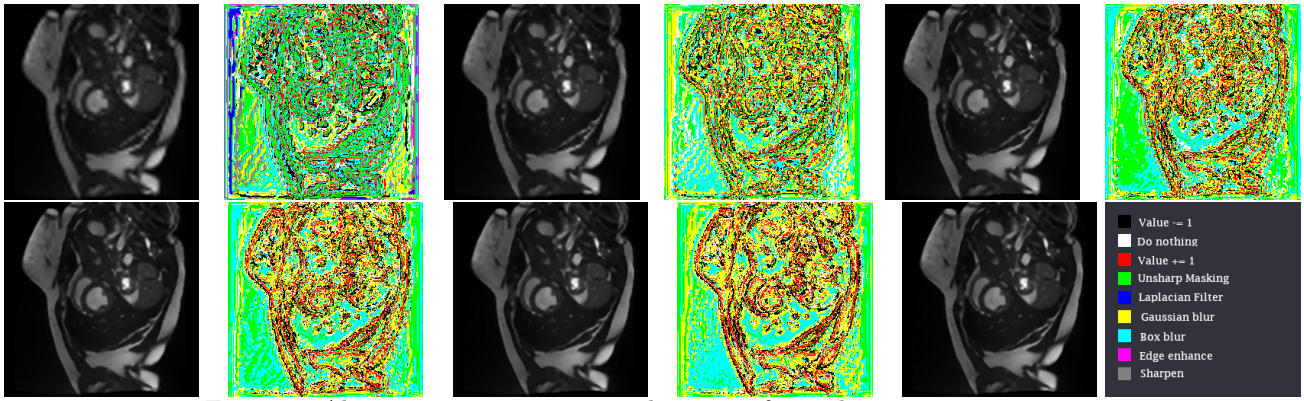

Figure 2: Alternating action maps and outputs for each processing time step

The previously existing RL implementation for image enhancement on GitHub[24] did not include processes to output action maps, save intermediary processing steps, evaluate images on metrics other than PSNR, nor the ability to choose which images were saved to disk. The previous implementation also used a pre-trained model for denoising as their initial weights which were removed in the proposed method.

3. RESULTS

Table 1: Image quality measures calculated for slices of the ADNI dataset, the values indicate the mean ± the standard deviation.

ADNI data set				
Measure	Pixel-RL	Bicubic interpolation	Bilinear interpolation	Unsharp masking
MAE	**2.29 ± 1.07**	2.91 ± 1.34	3.40 ± 1.57	3.47 ± 1.70
NRMSE	**0.19 ± 0.17**	0.24 ± 0.23	0.28 ± 0.29	0.24 ± 0.14
PSNR	**30.55 ± 3.11**	28.79 ± 3.08	27.87 ± 3.16	27.54 ± 3.34
SSIM	**0.96 ± 0.02**	0.94 ± 0.03	0.92 ± 0.04	0.94 ± 0.03
VIF	**0.39 ± 0.03**	0.31 ± 0.03	0.28 ± 0.02	0.28 ± 0.02

Table 2: Image quality measures calculated for slices of the BraTS dataset, the values indicate the mean ± the standard deviation.

BRATS data set				
Measure	Proposed	Bicubic interpolation	Bilinear interpolation	Unsharp masking
MAE	**1.28 ± 0.54**	1.90 ± 0.79	2.31 ± 0.96	2.35 ± 1.04
NRMSE	**0.09 ± 0.11**	0.14 ± 0.17	0.16 ± 0.22	0.14 ± 0.11
PSNR	**34.61 ± 2.47**	31.09 ± 2.77	29.95 ± 2.82	30.00 ± 2.74
SSIM	**0.97 ± 0.01**	0.96 ± 0.02	0.94 ± 0.02	0.95 ± 0.02
VIF	**0.51 ± 0.04**	0.40 ± 0.04	0.36 ± 0.04	0.35 ± 0.03

The action maps demonstrate that the model uses the full range of its action space in addition to focusing on enhancing edges. The model was then evaluated on two external datasets. The Alzheimer's Disease Neuroimaging Initiative (ADNI) dataset (3,610 images),[29] and a subset of the Multimodal Brain Tumor Segmentation (BraTS) dataset[30] (3,933 images), where blank images were removed, and all images were zero-padded to fit 256×256. Our implementation required just over 5.1 hours to train over 16,384 episodes. Testing external datasets took approximately 10 minutes each, or roughly 0.15 seconds per image. This work was performed on WSL2, Ubuntu 20.04.4 LTS with CUDA version 10.1.243 on NVIDIA RTX 3070, Intel i7-9700K, and given 7 GB of DIMM memory. For quantitative comparison, we used various evaluation measures: Peak Signal to Noise Ration

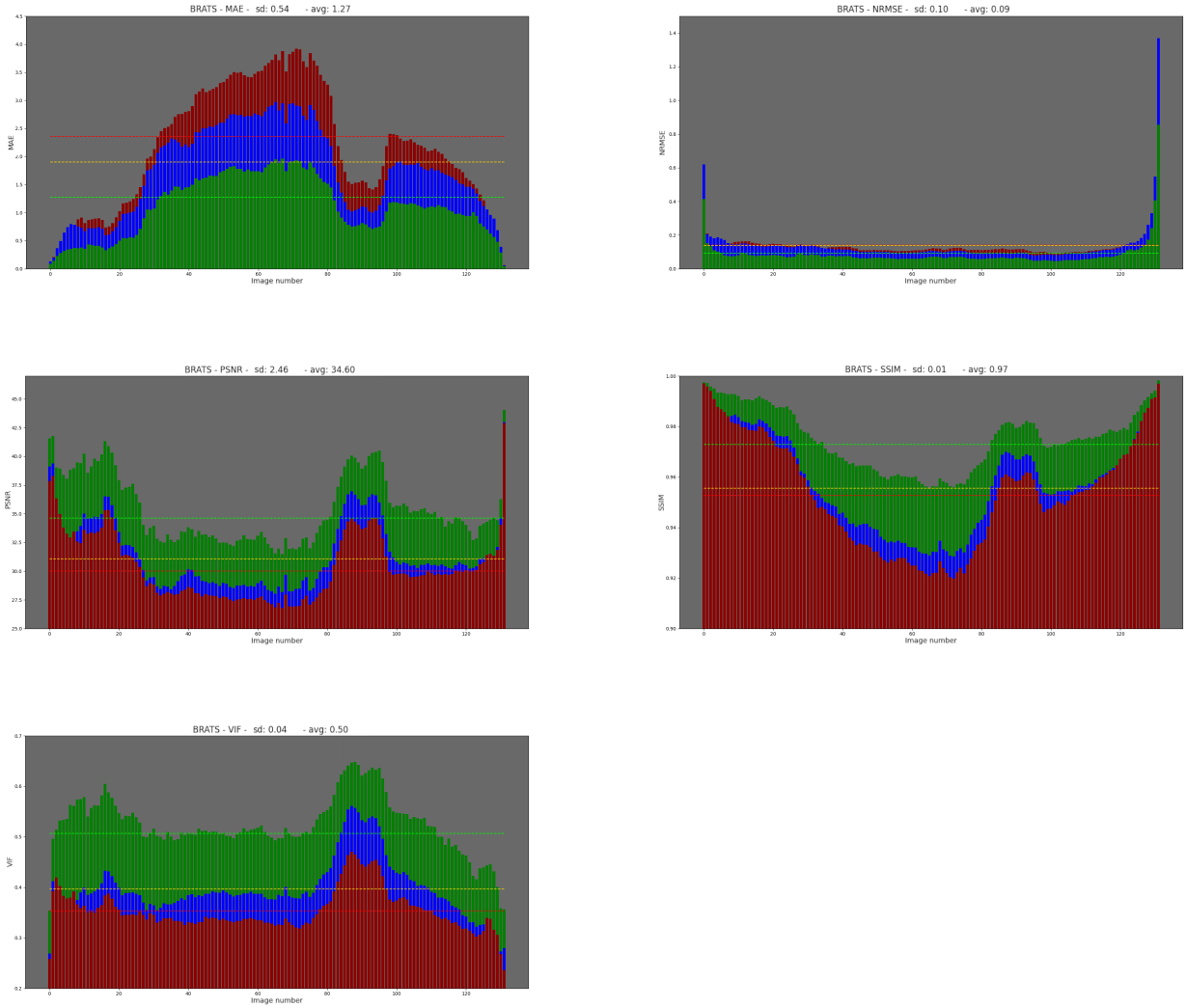

Figure 3: Various metrics evaluated over a single subject from the BraTS dataset by slice. Averages and standard deviations are calculated over the entire dataset and are shown for reference. Red: input, Blue: result of unsharp masking, Green: Proposed SR output.

(PSNR), Structural Similarity Index (SSIM), Mean Absolute Error (MAE), Normalized Root Mean Square Error (NRMSE), and Visual information fidelity (VIF), see Figure 3.

As shown in Tables 1 and 2, by all metrics (calculated using signal intensity values) the model produced superior quantitative results compared to the initial bicubic input as well as over any singular operator. Qualitative examples can also be seen in Figures 4 and 5. A comparison could not be made with the base implementation, Pixel-RL, because their focus was on de-blurring rather than SISR. Furthermore, a comparison could not be made with the SISR-focused Pixel-RL model,[22] Pixel-RL-SR, because the GANs used were not configured towards medical imagery. Our code is publicly available at https://github.com/Alix-B/PixelRL-SR-Local.

4. CONCLUSIONS

In conclusion, our model indicates that pixel-wise local operators provide promising results to enhance the spatial resolution of input images. We envision that our method could be used to accurately distinguish pixels belonging to potentially pathological lesions from those in healthy tissues especially at the interface of these zones, leading

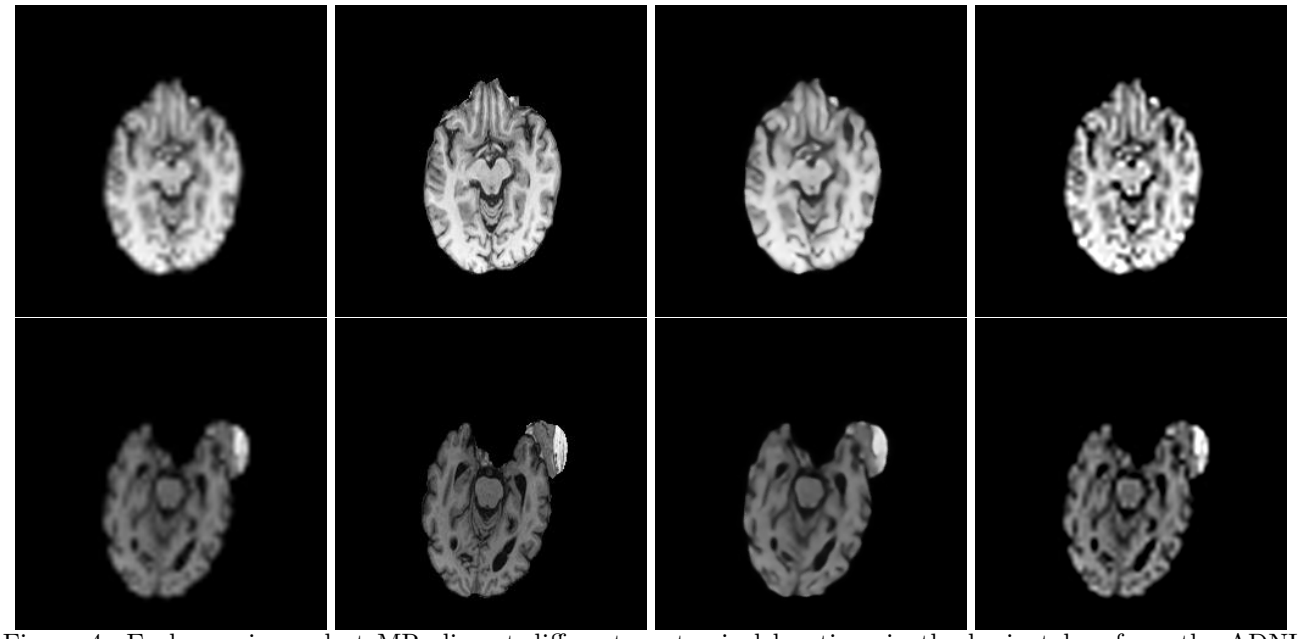

Figure 4: Each row is a select MR slice at different anatomical locations in the brain taken from the ADNI dataset. From left to right: Input image (Bicubic), Ground truth, Proposed, Unsharp masking

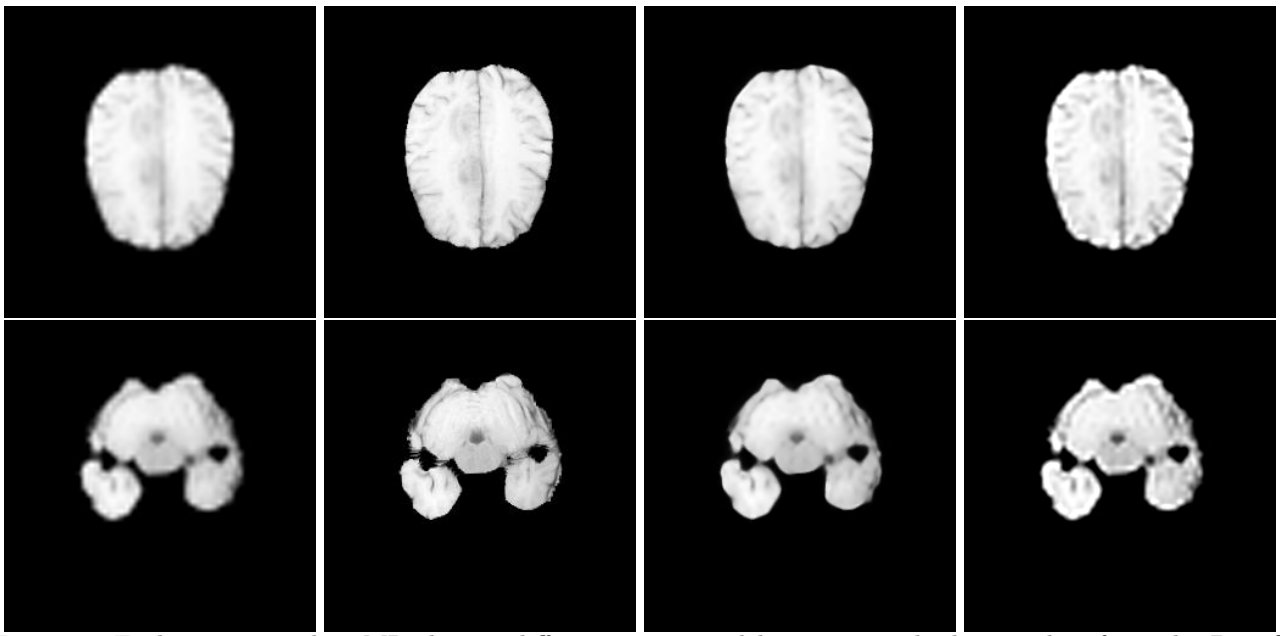

Figure 5: Each row is a select MR slice at different anatomical locations in the brain taken from the BraTS dataset. From left to right: Input image (Bicubic), Ground truth, Proposed, Unsharp masking

to more effective local therapies. The proposed method produces visually comparable results to SISR-specific algorithms such as Real-ESRGAN.[18]

Acknowledgements

This research was supported in part by the Natural Sciences and Engineering Research Council of Canada.

REFERENCES

[1] Duchon, C. E., "Lanczos filtering in one and two dimensions," *Journal of Applied Meteorology and Climatology* **18**(8), 1016–1022 (1979).

[2] Nguyen, N. X., *Numerical Algorithms for Image Superresolution*, PhD thesis, Graduate Program in Scientific Computation and Computational Mathematics, Stanford University (July 2000).

[3] Makwana, R. R. and Mehta, N. D., "Survey on Single image Super Resolution Techniques," *IOSR Journal of Electronics and Communication Engineering* **5**(5), 23–33 (2013).

[4] Freeman, W. T., Jones, T. R., and Pasztor, E. C., "Example-based super-resolution," *IEEE Computer Graphics and Applications* **22**(2), 56–65 (2002).

[5] Elad, M. and Datsenko, D., "Example-based regularization deployed to super-resolution reconstruction of a single image," *The Computer Journal* **50**(4), 1–16 (2007).

[6] Farsiu, S., Robinson, D., Elad, M., and Milanfar, P., "Advances and challenges in super-resolution," *International Journal of Imaging Systems and Technology* **14**, 47–57 (August 2004).

[7] Chaudhuri, S., [*Super-Resolution Imaging*], Kluwer, Boston, MA (2001).

[8] Ebrahimi, M. and Vrscay, E. R., "Solving the inverse problem of image zooming using "self-examples"," in [*International Conference Image Analysis and Recognition*], 117–130, Springer (2007).

[9] Ebrahimi, M. and Vrscay, E. R., "Multi-Frame Super-Resolution with No Explicit Motion Estimation.," *Proceedings of the International Conference on Image Processing, Computer Vision, and Pattern Recognition, IPCV.* , 455–459 (2008).

[10] Glasner, D., Bagon, S., and Irani, M., "Super-resolution from a single image," in [*2009 IEEE 12th International Conference on Computer Vision (ICCV)*], 349–356, IEEE (2009).

[11] Ebrahimi, M. and Bohun, S., "Single image super-resolution via non-local normalized graph Laplacian regularization: A self-similarity tribute," *Communications in Nonlinear Science and Numerical Simulation* **93**, 105508 (2021).

[12] Ebrahimi, M. and Vrscay, E. R., "Multi-frame super-resolution with no explicit motion estimation.,"

[13] Nazeri, K., Thasarathan, H., and Ebrahimi, M., "Edge-informed single image super-resolution," in [*Proceedings of the IEEE/CVF International Conference on Computer Vision Workshops*], 0–0 (2019).

[14] Ebrahimi, M. and Vrscay, E. R., "Nonlocal-means single-frame image zooming," in [*PAMM: Proceedings in Applied Mathematics and Mechanics*], **7**(1), 2020067–2020068, Wiley Online Library (2007).

[15] Ebrahimi, M., Vrscay, E. R., and Martel, A. L., "Coupled multi-frame super-resolution with diffusive motion model and total variation regularization," in [*2009 International Workshop on Local and Non-Local Approximation in Image Processing*], 62–69, IEEE (2009).

[16] Ebrahimi, M. and Martel, A. L., "A PDE approach to coupled super-resolution with non-parametric motion," in [*International Workshop on Energy Minimization Methods in Computer Vision and Pattern Recognition*], 112–125, Springer (2009).

[17] Abedjooy, A. and Ebrahimi, M., "Multi-modality image super-resolution using generative adversarial networks," *arXiv preprint arXiv:2206.09193* (2022).

[18] Rashid, S. I., Shakibapour, E., and Ebrahimi, M., "Single MR image super-resolution using generative adversarial network," *arXiv preprint arXiv:2207.08036* (2022).

[19] Goodfellow, I., Pouget-Abadie, J., Mirza, M., Xu, B., Warde-Farley, D., Ozair, S., Courville, A., and Bengio, Y., "Generative adversarial networks," *Communications of the ACM* **63**(11), 139–144 (2020).

[20] Ledig, C., Theis, L., Huszár, F., Caballero, J., Cunningham, A., Acosta, A., Aitken, A., Tejani, A., Totz, J., Wang, Z., et al., "Photo-realistic single image super-resolution using a generative adversarial network," in [*Proceedings of the IEEE conference on computer vision and pattern recognition*], 4681–4690 (2017).

[21] Vassilo, K., Heatwole, C., Taha, T., and Mehmood, A., "Multi-step reinforcement learning for single image super-resolution," in [*2020 IEEE/CVF Conference on Computer Vision and Pattern Recognition Workshops (CVPRW)*], 2160–2168 (2020).

[22] Nhat-Thanh, "Pixel-RL-SR Github, https://github.com/nhat-thanh/pixelrl-sr," (2020).

[23] Furuta, R., Inoue, N., and Yamasaki, T., "Fully convolutional network with multi-step reinforcement learning for image processing," in [*AAAI Conference on Artificial Intelligence (AAAI)*], (2019).

[24] Furuta, R., Inoue, N., and Yamasaki, T., "Pixelrl: Fully convolutional network with reinforcement learning for image processing," *IEEE Transactions on Multimedia (TMM)* **22**(7), 1704–1719 (2020).

[25] Li, Y., Sixou, B., and Peyrin, F., "A review of the deep learning methods for medical images super resolution problems," *Ingénierie et recherche biomédicale* **42**(2), 120–133 (2021).

[26] Greenspan, H., "Super-resolution in medical imaging," *Computer journal* **52**(1), 43–63 (2009).

[27] Bouffard, A., "Pixel-RL-Local Github, https://github.com/alix-b/pixelrl-sr-local," (2022).

[28] Bernard, O., Lalande, A., Zotti, C., Cervenansky, F., Yang, X., Heng, P.-A., Cetin, I., Lekadir, K., Camara, O., Ballester, M. A. G., et al., "Deep learning techniques for automatic MRI cardiac multi-structures segmentation and diagnosis: is the problem solved?," *IEEE transactions on medical imaging* **37**(11), 2514–2525 (2018).

[29] Jack Jr, C. R., Bernstein, M. A., Fox, N. C., Thompson, P., Alexander, G., Harvey, D., Borowski, B., Britson, P. J., L. Whitwell, J., Ward, C., et al., "The Alzheimer's disease neuroimaging initiative (ADNI): MRI methods," *Journal of Magnetic Resonance Imaging: An Official Journal of the International Society for Magnetic Resonance in Medicine* **27**(4), 685–691 (2008).

[30] Menze, B. H., Jakab, A., Bauer, S., Kalpathy-Cramer, J., Farahani, K., Kirby, J., Burren, Y., Porz, N., Slotboom, J., Wiest, R., et al., "The multimodal brain tumor image segmentation benchmark (BRATS)," *IEEE transactions on medical imaging* **34**(10), 1993–2024 (2014).